nature chemistry

ARTICLES

PUBLISHED ONLINE: 18 DECEMBER 2017 | DOI: 10.1038/NCHEM.2905

Substrate-driven chemotactic assembly in an enzyme cascade

Xi Zhao[1†], Henri Palacci[2†], Vinita Yadav[1], Michelle M. Spiering[1], Michael K. Gilson[3], Peter J. Butler[4], Henry Hess[2*], Stephen J. Benkovic[1*] and Ayusman Sen[1*]

Enzymatic catalysis is essential to cell survival. In many instances, enzymes that participate in reaction cascades have been shown to assemble into metabolons in response to the presence of the substrate for the first enzyme. However, what triggers metabolon formation has remained an open question. Through a combination of theory and experiments, we show that enzymes in a cascade can assemble via chemotaxis. We apply microfluidic and fluorescent spectroscopy techniques to study the coordinated movement of the first four enzymes of the glycolysis cascade: hexokinase, phosphoglucose isomerase, phosphofructokinase and aldolase. We show that each enzyme independently follows its own specific substrate gradient, which in turn is produced by the preceding enzymatic reaction. Furthermore, we find that the chemotactic assembly of enzymes occurs even under cytosolic crowding conditions.

The interaction between enzymes in living cells is an area of active research. In many instances, enzymes that participate in reaction cascades have been shown to assemble into metabolons in response to the presence of the initial substrate to facilitate substrate channelling[1–3]. Substrate channelling promotes sequential reactions with high yield and high selectivity by directing reaction intermediates along a specific pathway from one enzyme to the next. Inspired by these biological cascade reactions, multicatalyst nanostructures have been fabricated for efficient chemical synthesis[4–6]. There are several suggested mechanisms for biological metabolon formation and substrate channelling. Some involve stable protein–protein interactions[7,8], while others invoke electrostatic guidance[9,10] or spatial organization and clustering[11,12]. In other cases, metabolon formation through reversible and/or post-translational modifications has been suggested, but such transient complexes have eluded isolation[13,14]. Recently, the diffusive motion of enzymes has been shown to increase as a function of substrate concentration and reaction rate; furthermore, active enzymes migrate up the substrate gradient, an example of molecular chemotaxis[15–17]. Here, we present evidence that suggests that enzymes along a metabolic pathway in which the product of one is the substrate for the next tend to associate through a process of sequential, directed chemotactic movement. Such a process may contribute to the formation of metabolons in living cells co-localized around mitochondria (which serve as sources of adenosine triphosphate, ATP)[18].

Our experimental study applies microfluidic and fluorescence spectroscopy techniques to study the coordinated movement of hexokinase (HK) and aldolase (Ald), the first and fourth enzymes of the glycolysis cascade, which are connected by the intermediate enzymes phosphoglucose isomerase (Iso) and phosphofructokinase (PFK) (Fig. 1a). Metabolon formation by glycolytic enzymes has been suggested in the literature[19]. To monitor the movement of HK and Ald by confocal microscopy, we fluorescently labelled them with distinct amine-reactive (excitation/emission at 493 and 518 nm) and thiol-reactive (638 and 658 nm) Dylight dyes, respectively. The use of different dyes enables simultaneous measurement of both enzymes in microfluidic experiments. For both HK and Ald, a linear relationship was observed between fluorescence intensity and concentration (Supplementary Fig. 1). This allowed us to estimate the amount of enzyme migrating into a specific substrate channel.

Results and discussion

Catalysis-induced enhanced diffusion of HK and Ald. Before examining the effect of an imposed substrate gradient on the movement of HK and Ald, we measured their diffusion coefficients in uniform substrate concentrations by fluorescence correlation spectroscopy (FCS). The diffusion constants of both enzymes rise with increasing substrate concentration, saturating at increases of 38% for HK and 35% for Ald (Supplementary Fig. 2). As previously reported[15–17,20–22], the substrate-induced increase in the diffusion constant is proportional to the catalytic velocity computed from known Michaelis–Menten parameters.

Individual enzyme chemotaxis. To examine the chemotactic movement of enzymes in response to a substrate gradient, a three-inlet/one-outlet microfluidic flow device was fabricated by photolithography (Fig. 1b). With known fluid flow rates and channel geometries, the distance from the input points to the measurement line can be converted into the time available for the enzymes to react and diffuse (Supplementary Table 1). As a control experiment, HK (200 nM), D-glucose (50 mM) and $MgCl_2$ (100 mM) were passed through all three channels. The solution in the central channel was then changed to HK (200 nM), D-glucose (50 mM), $MgCl_2$ (100 mM) and ATP (50 mM). NaCl (150 mM) was added into the two flanking channels to balance the ionic strength of the ATP disodium salt added to the centre channel. As shown in Fig. 2, we observed significant enzyme 'focusing' in the central channel following an interaction time of 34.6 s in the microchannel, compared to when ATP was absent. The total fluorescence intensity in all the experiments was normalized to 1

[1]Department of Chemistry, The Pennsylvania State University, University Park, Pennsylvania 16802, USA. [2]Department of Biomedical Engineering, Columbia University, New York, New York 10027, USA. [3]Skaggs School of Pharmacy and Pharmaceutical Sciences, University of California, San Diego, La Jolla, California 92093, USA. [4]Department of Biomedical Engineering, The Pennsylvania State University, University Park, Pennsylvania 16802, USA. †These authors contributed equally to this work. *e-mail: hhess@columbia.edu; sjb1@psu.edu; asen@psu.edu

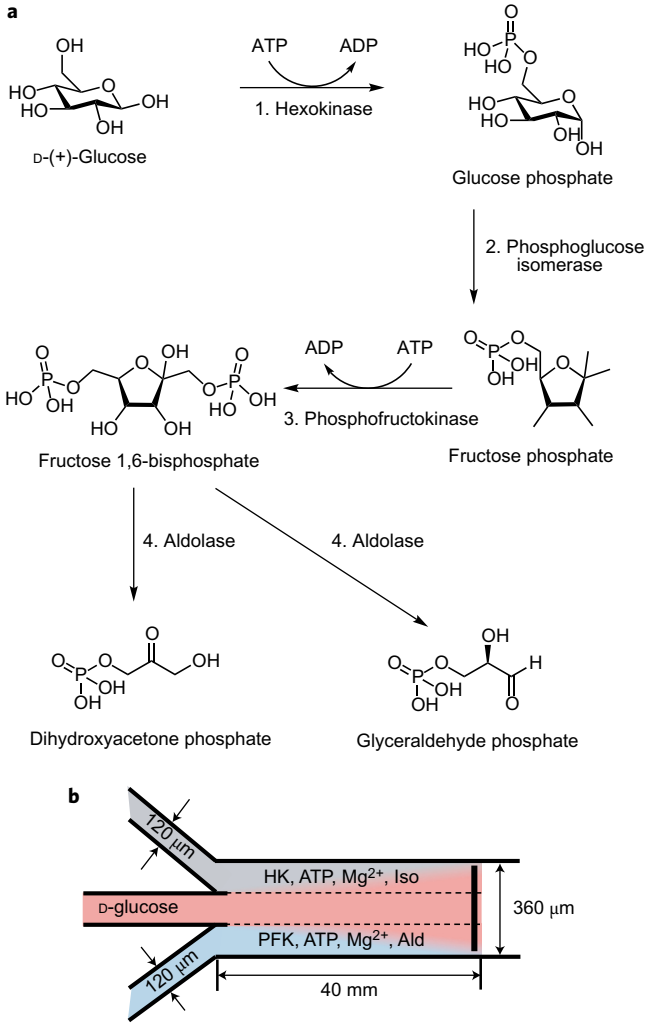

Figure 1 | Studied enzymatic reactions and microfluidic device. a, First four steps of glycolysis and their associated enzymes: hexokinase (HK), phosphoglucose isomerase (Iso), phosphofructokinase (PFK) and aldolase (Ald). **b**, Photolithographically fabricated flow-based microfluidic channel for studying enzyme chemotaxis (channel length, 40 mm; width, 360 μm; depth, 100 μm). Due to laminar flow, the effective width of each flow channel is 120 μm. Fluorescence intensities were analysed across the combined channel where indicated by the vertical black line, except for 20 μm next to the sidewalls.

for comparison and representation on a common scale. We repeated the experiment substituting mannose, a substrate that binds more strongly but is turned over more slowly by HK, and found that the enzyme focused less than in the presence of D-glucose. We also repeated the experiment substituting L-glucose, the enantiomer of D-glucose that is not a substrate, and observed no focusing. Similarly, the substitution of ATP by its analogue AMP-PCP (adenosine 5′-(β,γ-methylene) triphosphate) at the same concentration in the central channel resulted in no focusing. Note that both ATP and AMP-PCP bind to HK, but the latter cannot turn over and phosphorylate glucose[23]. As expected, the extent of focusing for D-glucose decreased under otherwise identical conditions when the interaction time in the middle channel was reduced (Supplementary Fig. 3).

We propose that the chemotactic aggregation of enzymes in regions of high substrate concentrations is due to cross-diffusion effects[24]. The substrate gradient-induced aggregation by cross-diffusion counteracts Fickian diffusion of enzymes, which transfers enzymes from regions with high enzyme concentration to regions with low enzyme concentration. Cross-diffusion is different from the enhanced diffusion of an enzyme in the presence of its substrate[15–17,20–22], which is also observed for uniform substrate concentrations and accelerates the equilibration of the enzyme concentration by Fickian diffusion. The complete theoretical description of diffusion in a multicomponent system combines the flow of a species in proportion to its concentration gradient (Fick's law) and the flow of the same species in response to the concentration gradients of other species in solution. The diffusive flow for a concentration c_e of unbound enzyme E in the presence of its substrate S can then be written as

$$J_e = -D\nabla c_e - D_{XD}\nabla c_s \quad (1)$$

where D is the Fick's law diffusion coefficient, D_{XD} is the 'cross-diffusion' coefficient, and ∇c_e and ∇c_s are gradients in the enzyme and substrate concentrations, respectively. Cross-diffusive effects have been experimentally measured in ternary reaction–diffusion systems[24], protein–electrolyte solutions[25], protein–polymer solutions[26] and in many other systems[27]. We followed the theory of chemotaxis originating from short-range ligand binding proposed by Schurr *et al.*[28] to obtain the cross-diffusion coefficient D_{XD} as a function of local substrate concentration c_s, diffusion coefficient D, computed from the Einstein relation ($70\ \mu m^2\ s^{-1}$ for the HK–glucose complex) and the equilibrium constant K of ATP binding to the enzyme ($5 \times 10^3\ M^{-1}$ for the binding of ATP to HK–glucose[29]):

$$D_{XD} = -Dc_e \frac{K}{1 + Kc_s} \quad (2)$$

Inserting equation (2) into equation (1) shows the factors driving cross-diffusion flow:

$$J_e = -D\left(\nabla c_e - c_e \frac{K}{1 + Kc_s}\nabla c_s\right) \quad (3)$$

The first term inside the parentheses is traditional diffusion towards lower concentrations of enzyme. The second term's sign is opposite, showing that this flow is towards a higher concentration of substrate. In addition to the substrate gradient, this term's magnitude is determined by three factors: diffusion coefficient D, enzyme concentration c_e and a factor proportional to the fraction of binding sites occupied by the substrate at a given time. As with Fickian diffusion, the cross-diffusion drift arises from a thermodynamic driving force that lowers the chemical potential of the system due to favourable enzyme–substrate binding.

The system of partial differential equations corresponding to the HK–glucose catalysis reaction diffusion system has been solved numerically (see Supplementary Section 'Computational modelling of cross-diffusion'). The initial presence of ATP in the central channel gives rise to strong ATP gradients at the boundaries between the central channel and the left and right channels. The D-glucose, present in all channels, converts HK to the HK–glucose complex, which is the cross-diffusing entity described by equation (3). Without any adjustable parameters and without accounting for catalysis-induced enhanced diffusion, the model predicts focusing lower than that seen in experiments, but with the same direction and order of magnitude (Fig. 3). Thus, HK will chemotax up an ATP gradient due to the cross-diffusion phenomenon. One reason for the difference between experiment and theory is enhanced diffusion of the enzymes in the presence of catalysis; increased D will increase the amount of focusing, as predicted by the model. However, because there is no established theoretical framework for the

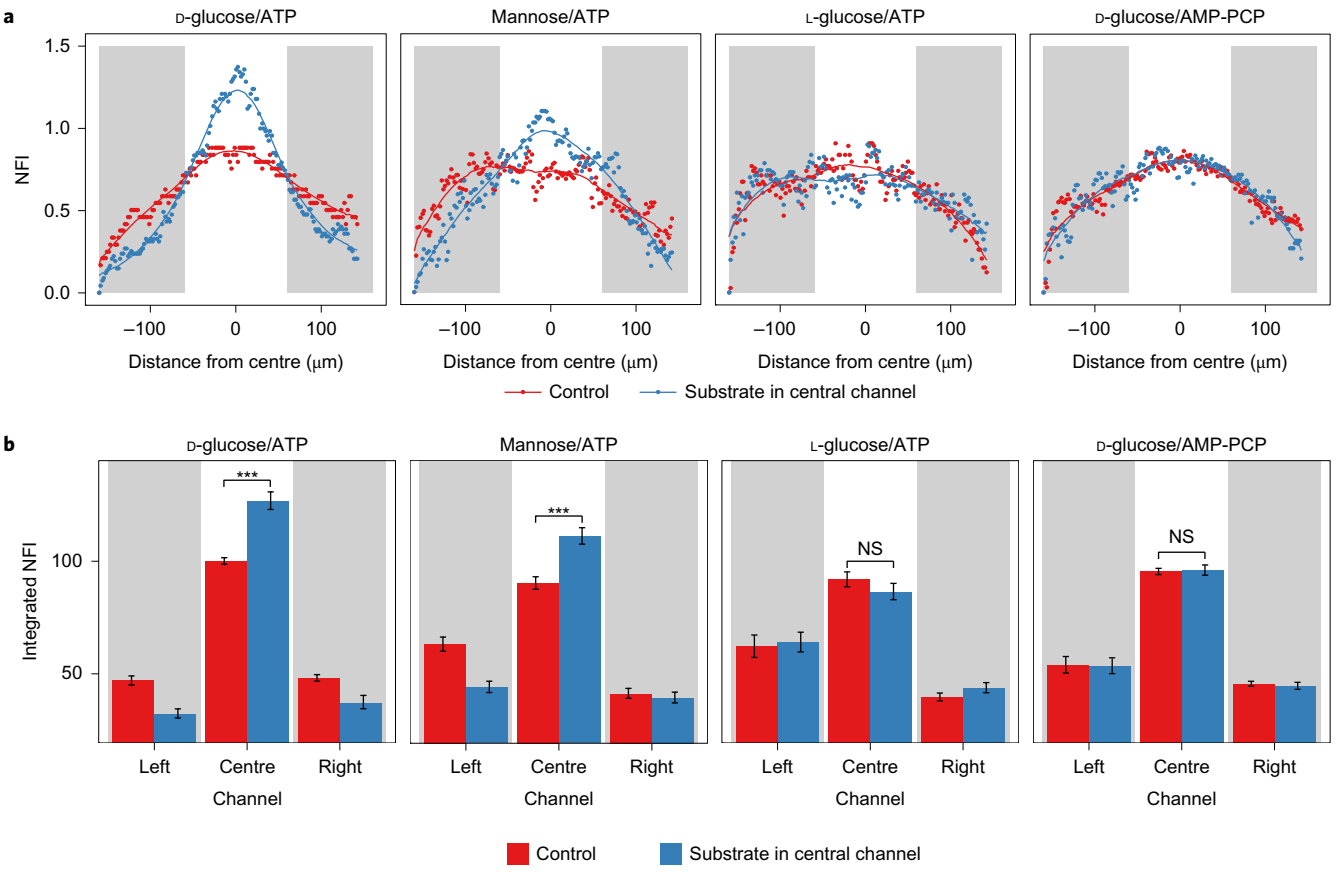

Figure 2 | Catalysis-induced enzyme focusing. A starting equilibrium distribution of HK (200 nM), D-glucose (50 mM) and $MgCl_2$ (100 mM) shows focusing towards the middle channel when ATP (50 mM) is introduced into it. Note that catalysis does not occur in the absence of ATP (control). Experimental conditions: flow rate, 50 μl h^{-1}; distance, 38 mm; interaction time, 34.6 s. The general concave shape of the curves is indicative of the wall effect. **a**, Normalized fluorescence intensity (NFI) averaged across three experiments as a function of distance from the centre of the channel. Fluorescence intensities are normalized across all channels such that the total fluorescence intensity across all channels is fixed for all experiments and rescaled such that the central channel for the D-glucose control experiment sums to 100. Side channels are shaded in grey. Data points are locally fitted to a second degree polynomial (see Supplementary Section 'Statistical analysis of experimental results'). **b**, Integrated NFI per channel averaged over three experiments. Error bars are 95% confidence intervals obtained from 500 bootstrap iterations of the fitting process. A pairwise *t*-test with Holm adjustment was conducted to test for significant differences in the intensities across channels. The pairwise *t*-test for the sum of the left and right channels would give the same results because the total fluorescence across the three channels is normalized for each experiment. ***$P < 0.001$; NS, not significant.

determination of D as a function of position across the microfluidic channel, we have not included it in our model.

We also modelled the focusing experiment in the presence of the non-hydrolysable ATP analogue AMP-PCP, and found that the model predicts reduced focusing compared to the ATP-induced focusing (around 1% increase in the concentration in the central channel; see Supplementary Section 'Computational modelling of cross-diffusion' and Supplementary Fig. 6). The significantly stronger binding of AMP-PCP reduces the concentration c_e of unbound enzyme[30] and thereby the cross-diffusion effect. This suggests that the model is also compatible with the results for the AMP-PCP experiment, in which little focusing was observed.

Role of catalysis in chemotaxis. To confirm the role of substrate turnover in the observed chemotaxis, HK was exposed to its usual substrate, D-glucose, and mannose, a competitive substrate, as well as L-glucose, which is not a substrate. HK shows a higher binding affinity towards mannose than to D-glucose ($K_m = 40$ μM versus 120 μM). On the other hand, pyruvate kinase/lactate dehydrogenase coupled assays for HK activity confirmed mannose phosphorylation to be half as fast as D-glucose phosphorylation under similar reaction conditions (see Supplementary Section 'Enzyme activity assays'). In the experiments, the flow rate in each port was set to 200 μl h^{-1} and the fluorescence was measured 30 mm down the channel, allowing for a total diffusion/interaction time of 6.5 s. Buffer containing 200 nM HK, 10 mM ATP and 10 mM $MgCl_2$ was flowed through the middle channel while one flanking channel contained buffer with 10 mM D-glucose, buffer with 10 mM mannose or buffer with 10 mM L-glucose and the other channel contained buffer only, as a control. A significantly higher chemotactic shift was observed towards the D-glucose channel compared to the mannose channel (Fig. 4), suggesting that catalysis, rather than simple substrate binding, is important for the observed enzyme transport[31]. Although cross-diffusion itself only requires substrate binding, the diffusion coefficient controlling the magnitude of this effect will be significantly affected by catalysis through the enhanced diffusion mechanism. Equations (2) and (3) show that the cross-diffusion coefficient D_{XD} is directly proportional to the enzyme's diffusion coefficient D. The magnitude of the enzyme's diffusion coefficient is therefore one of the determining factors of enzyme chemotaxis and focusing. To further underscore the role of catalysis, a simplified model for cross-diffusion is discussed in Supplementary Section 'Simplified model for cross-diffusion illustrating the role of catalysis'. This illustrates that (1) the cross-diffusion phenomenon is dependent on the number of forward binding events in the region where the substrate gradient

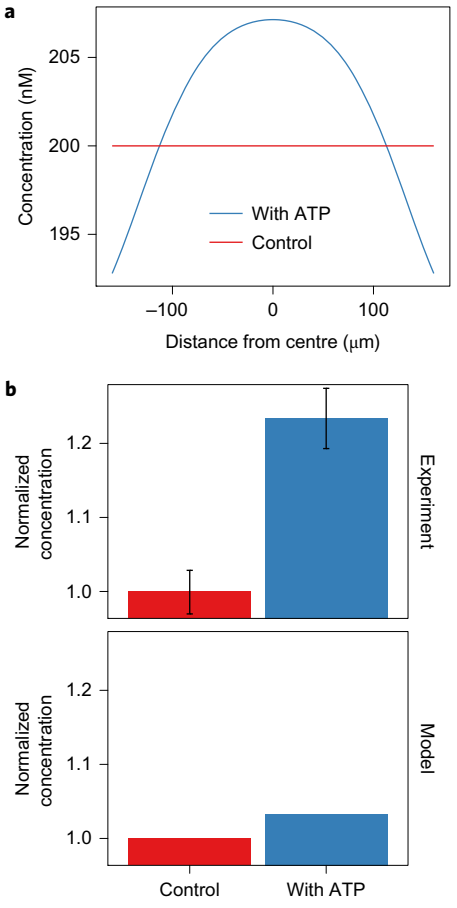

Figure 3 | Catalysis-induced enzyme focusing and computed profiles of total enzyme concentration replicating experimental conditions from Fig. 2. **a**, Modelled chemotactic response of HK in the presence of ATP, which is consistent with the experimental result (see Supplementary Section 'Computational modelling of cross-diffusion'). Parameters were chosen to replicate the conditions of the experiment described in Fig. 2a. **b**, Comparison between experimental results and computational results for the integrated NFI of the enzyme in the central channel: experimental (top) and modelled (bottom) enzyme focusing in the presence and absence of ATP. The experimental figure is the average of three experimental trials. Error bars are 95% confidence intervals obtained from 500 bootstrap iterations of the fitting process.

has been established, and (2) the turnover induced by enzyme catalysis allows for orders of magnitude more binding events to take place. Therefore, the catalytic step is crucial in the observed enzyme focusing.

Chemotaxis as a factor in metabolon formation. Having demonstrated that HK undergoes chemotaxis up its substrate gradient, we next probed the chemotactic behaviour of the entire four-enzyme cascade. The first experiment was designed to examine the response of Ald towards its substrate, fructose 1,6-bisphosphate, generated from D-glucose by the successive actions of the first three enzymes. In the microfluidic device, the Ald was flowed through the middle channel. The first three enzymes (HK, Iso and PFK), with Mg^{2+} and ATP (required by the kinases), were passed through one of the flanking channels together with 10 mM D-glucose, while buffer was passed through the flanking channel on the opposite side. The volumetric flow rate per inlet was fixed at 50 μl h^{-1}, allowing for a total interaction time of 17.3 s in a 20-mm-long channel. In total, 11.9 ± 3.0% of the Ald moved into the channel where its substrate was being formed *in situ* (Fig. 5a). When the interaction time was reduced to 8.6 s, the chemotactic migration correspondingly reduced to 4.9 ± 2.4% of the Ald. As expected, HK did not show any excess movement into the adjoining channel as compared with HK moving into a channel with buffer (Supplementary Fig. 4a). Additional control experiments were performed by removing either enzyme 2 (Iso), enzyme 3 (PFK) or

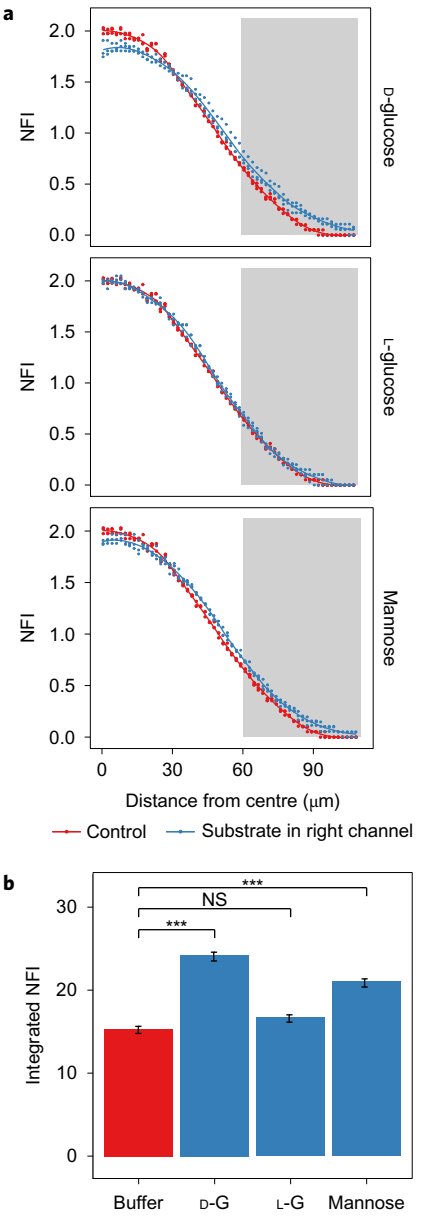

Figure 4 | Chemotactic shifts observed for HK in response to gradients of different substrates. HK shows a greater chemotactic shift towards its preferred substrate D-glucose compared to mannose, which it phosphorylates at a significantly lower rate. No chemotactic shift was observed with L-glucose. **a**, Experimental NFI in the central and right channels. All fluorescence intensities are normalized to a total of 1 across all channels, corresponding to a fixed total amount of enzyme in each experiment. **b**, Integrated NFI in the right channel. Experimental conditions: starting enzyme concentration = 200 nM (100%); flow rate = 200 μl h^{-1}; distance = 30 mm; interaction time = 6.5 s. The percentage of enzyme migration into the D-glucose channel is 7.3 ± 2.0% and into the mannose channel is 2.5 ± 1.2%, relative to buffer channel. Error bars are 95% confidence intervals. A pairwise *t*-test with Holm adjustment was conducted to test for significant differences in the intensities across channels. ***$P < 0.001$; NS, not significant.

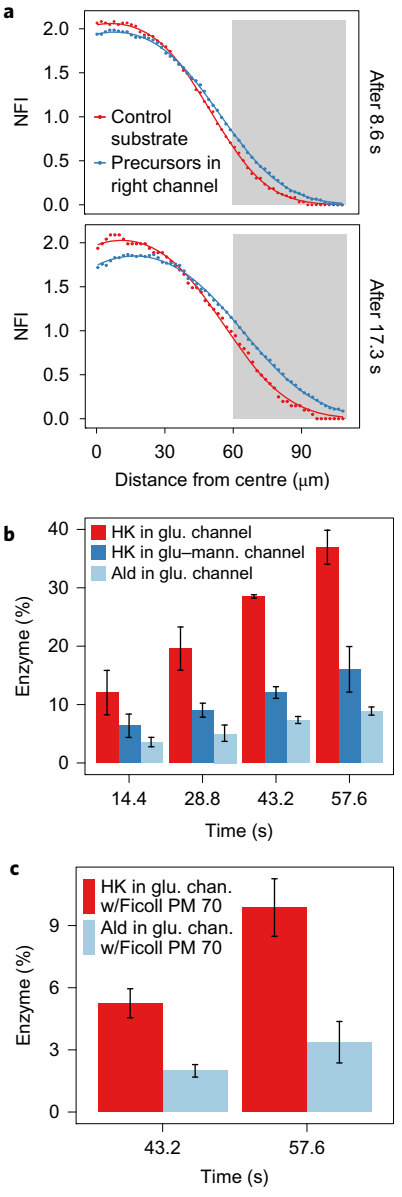

Figure 5 | Chemotactic assembly of enzymes in the microfluidic channel under different reaction conditions. a, Fluorescence intensity measured across the channels, plotted against width of the channels for the centre and right channels. The grey background represents the approximate right channel. When compared to the movement towards buffer, Ald shows enhanced migration into the channel that generates fructose-1,6-bisphosphate *in situ*. **b**, Ald shows a time-delayed chemotactic response compared to HK, as expected based on the sequence of reactions. When 10 mM mannose is introduced along with 10 mM D-glucose, HK shows a reduced chemotaxis corresponding to the slower rate of mannose phosphorylation by HK. Error bars are 95% confidence intervals. **c**, D-glucose gradient-driven sequential movement of HK and Ald for the entire enzymatic reaction cascade was also observed in the presence of Ficoll PM 70 (20% wt/vol), an induced crowded environment mimicking cytosolic conditions in a cell. Error bars are 95% confidence intervals.

D-glucose from the channel containing HK, Mg^{2+} and ATP. In each case, Ald showed no discernible chemotactic movement (Supplementary Fig. 4b). We then sought to examine whether there was a sequential spreading of HK and Ald when exposed to D-glucose. This is expected because D-glucose is the substrate for HK, while the substrate for Ald, fructose 1,6-bisphosphate, is only formed from D-glucose through three successive enzymatic steps. The components of the cascade were now separated into two batches consisting of the first two and last two enzymes, respectively. HK, ATP, Mg^{2+} and Iso were flowed through one flanking channel, while PFK, ATP, Mg^{2+} and Ald were flowed through the other flanking channel. A solution of D-glucose was passed through the middle channel. The flow rate was reduced to 30 μl h^{-1} and the channel length was increased to 40 mm, allowing for a total interaction time of 57.6 s within the channel. An examination of the enzyme reaction rates confirmed that the time available within the microchannel was sufficient for the entire cascade of reactions to occur (Supplementary Fig. 5). As discussed, we hypothesized that HK should respond first to its substrate gradient by moving into the D-glucose channel, thereby producing the substrate for enzyme 2 (Iso). The cascade would continue with PFK participation, finally producing fructose 1,6-bisphosphate, which in turn should prompt Ald to chemotax towards the central channel. The fluorescence profiles for enzymes HK and Ald were noted at different interaction times (14.4, 28.8, 43.2 and 57.6 s) and their chemotactic behaviour summarized in Fig. 5b and Supplementary Table 2. For HK, our results indicate that, in 57.6 s, 37.0 ± 0.3% of the starting 200 nM enzyme moves into the central channel containing D-glucose (10 mM), compared to 6.7 ± 1.3% of the enzyme moving into the same channel when flowing only buffer. The corresponding numbers for Ald are 8.9 ± 0.7% and 5.9 ± 1.0%, respectively (Supplementary Table 2). Thus, a sequential movement of HK, followed by Ald, towards the central channel was observed. We also observed a sequential movement of the two enzymes when we added mannose to D-glucose. Because mannose binds more strongly to HK but turns over more slowly, a smaller chemotactic shift is observed.

Effect of cytosolic crowding. To replicate the cytosolic crowding conditions that enzymes encounter in cells due to the presence of other macromolecules, we added 20% wt/vol Ficoll PM 70 to our experiments involving the entire cascade. Ficoll PM 70 is a highly branched polysaccharide polymer that serves as a synthetic crowding agent by affecting the fluidic properties of the solution, such as increasing the viscosity and osmolality[32]. As shown in Fig. 5c, the presence of the crowding agent slows down but does not stop the chemotactic movement of the enzymes.

Co-localization of HK and Ald. With the same crowding conditions and enzymes as used in the microfluidic experiments, we observed the co-localization of HK and Ald enzyme aggregates in a sealed hybridization chamber starting with a uniform distribution of all four enzymes in the cascade, as well as the substrates for HK (Supplementary Scheme 1). In the presence of D-glucose and ATP, both the fluorescently labelled HK and Ald form bright moving spots. When the spots of HK and Ald with diameters ranging from 600 to 1,000 nm were tracked, the trajectories of the two enzymes were found to be highly correlated (Fig. 6 and Table 1). Similar experiments were also performed either with D-glucose but no Iso and PFK present, or substituting D-glucose with L-glucose, or with no glucose. As shown in Table 1, there were far fewer HK and Ald spots present. However, the above observations do not conclusively establish metabolon formation: the procedure only allows us to visualize very large enzyme aggregates, significantly larger than the size of typically reported metabolons. Unfortunately, current techniques cannot precisely locate and track rapidly diffusing smaller enzyme aggregates in solution.

Conclusions

Our results suggest that the observed assembly of enzymes participating in a cascade in response to the presence of the initial substrate can be a result of individual enzymes undergoing chemotaxis in

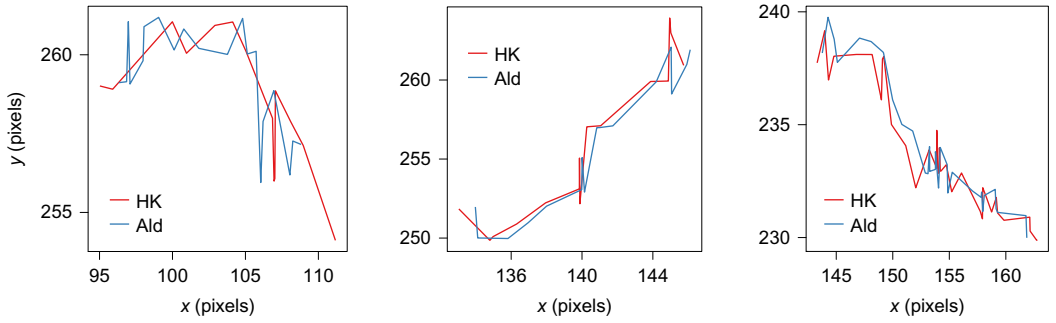

Figure 6 | Examples of HK and Ald trajectories from an experiment in which D-glucose and all four enzymes were present, for which the corresponding Ald trajectory was highly correlated. Experimental conditions: 200 nM HK labelled with amine-reactive (excitation/emission: 493/518 nm) Dylight dye; 200 nM Iso; 200 nM FPK; 200 nM Ald conjugated with thiol-reactive (excitation/emission: 638/658 nm) Dylight dye; 10 mM ATP; 20 mM $MgCl_2$; and 10 mM D-glucose in 20% wt/vol 70 M Ficoll mixed and injected into a sealed hybridization chamber (Supplementary Scheme 1). A pixel is 0.46 × 0.46 μm and the frame rate is 1 frame every 1.29 s. Trajectories are recorded for 10 frames, ~13 s.

Table 1 | Statistic of HK and Ald trajectories.

Experiment	Total HK trajectories	HK trajectories with high Ald correlation
D-Glucose with all four enzymes (eight experiments)	48 ± 3 (s.e.m.)	32 ± 2 (s.e.m.)
D-Glucose without Iso and PFK present (three experiments)	12 ± 2 (s.e.m.)	5 ± 1 (s.e.m.)
L-Glucose with all four enzymes (three experiments)	1	0
No glucose with all four enzymes (two experiments)	1	0

Total number of detected hexokinase (HK) trajectories and total number of HK trajectories found to be correlated with an aldolase (Ald) trajectory (correlation >95%). s.e.m., standard error of the mean.

response to their specific substrate gradients. We identified and quantified the two major effects explaining chemotaxis. First, in the case of HK, cross-diffusion up the ATP and glucose gradients is the main mechanism causing localization and is dependent on ATP and glucose binding. Second, the magnitude of the effect is increased by the enhanced diffusion effect, which we have shown to be dependent on catalysis, for HK, when both ATP and glucose are present. The extent of enzyme migration is proportional to time of exposure to the substrate gradient. The reduced chemotaxis with mannose, a less active substrate for HK, emphasizes the contribution of catalysis to the phenomenon. Significantly, the chemotactic migration of enzymes is fairly rapid even under conditions that mimic cytosolic crowding, a rate very similar to that reported for enzyme diffusion in living cells[33]. This phenomenon, chemotaxis, does not require direct interaction between the enzymes to form complexes that promote substrate channelling; metabolon formation could simply be triggered by the presence of an initial substrate gradient, for example ATP gradients near mitochondria in the case of the transient metabolon, the purinosome. Furthermore, the enzymes should revert back to their equilibrium distribution once the initial substrate is completely reacted and substrate gradients for the individual enzymes disappear. Presuming this phenomenon to be general[30], chemotaxis may be a basis for the organization of metabolic networks in the cytosol of the cell.

Data availability. The experimental and theoretical data that support the findings of this study are available from the corresponding authors upon request.

Received 9 December 2016; accepted 1 November 2017; published online 18 December 2017

References

1. Miles, E. W., Rhee, S. & Davies, D. R. The molecular basis of substrate channeling. *J. Biol. Chem.* **274,** 12193–12196 (1999).
2. Wheeldon, I. *et al.* Substrate channelling as an approach to cascade reactions. *Nat. Chem.* **8,** 299–309 (2016).
3. Lin, J.-L., Palomec, L. & Wheeldon, I. Design and analysis of enhanced catalysis in scaffolded multienzyme cascade reactions. *ACS Catal.* **4,** 505–511 (2014).
4. Yamada, Y. *et al.* Nanocrystal bilayer for tandem catalysis. *Nat. Chem.* **3,** 372–376 (2011).
5. Zhao, M. *et al.* Core–shell palladium nanoparticle@metal–organic frameworks as multifunctional catalysts for cascade reactions. *J. Am. Chem. Soc.* **136,** 1738–1741 (2014).
6. Zhang, Y. H. Substrate channeling and enzyme complexes for biotechnological applications. *Biotechnol. Adv.* **29,** 715–725 (2011).
7. An, S., Kumar, R., Sheets, E. D. & Benkovic, S. J. Reversible compartmentalization of *de novo* purine biosynthetic complexes in living cells. *Science* **320,** 103–106 (2008).
8. Nishi, H., Hashimoto, K. & Panchenko, A. R. Phosphorylation in protein–protein binding: effect on stability and function. *Structure* **19,** 1807–1815 (2011).
9. Lindbladh, C. *et al.* Preparation and kinetic characterization of a fusion protein of yeast mitochondrial citrate synthase and malate-dehydrogenase. *Biochemistry* **33,** 11692–11698 (1994).
10. Wu, F. & Minteer, S. Krebs cycle metabolon: structural evidence of substrate channeling revealed by cross-linking and mass spectrometry. *Angew. Chem. Int. Ed.* **54,** 1851–1854 (2015).
11. Winkel-Shirley, B. Evidence for enzyme complexes in the phenylpropanoid and flavonoid pathways. *Physiol. Plant.* **107,** 142–149 (1999).
12. Jorgensen, K. *et al.* Metabolon formation and metabolic channeling in the biosynthesis of plant natural products. *Curr. Opin. Plant. Biol.* **8,** 280–291 (2005).
13. Graham, J. W. A. *et al.* Glycolytic enzymes associate dynamically with mitochondria in response to respiratory demand and support substrate channeling. *Plant Cell* **19,** 3723–3738 (2007).
14. Campanella, M. E., Chu, H. & Low, P. S. Assembly and regulation of a glycolytic enzyme complex on the human erythrocyte membrane. *Proc. Natl Acad. Sci. USA* **102,** 2402–2407 (2005).
15. Sengupta, S. *et al.* Enzyme molecules as nanomotors. *J. Am. Chem. Soc.* **135,** 1406–1414 (2013).
16. Sengupta, S. *et al.* DNA polymerase as a molecular motor and pump. *ACS Nano* **8,** 2410–2418 (2014).
17. Yu, H., Jo, K., Kounovsky, K. L., Pablo, J. J. & Schwartz, D. C. Molecular propulsion: chemical sensing and chemotaxis of DNA driven by RNA polymerase. *J. Am. Chem. Soc.* **131,** 5722–5723 (2009).
18. French, J. B. *et al.* Spatial colocalization and functional link of purinosomes with mitochondria. *Science* **351,** 733–737 (2016).
19. Kohnhorst, C. L. *et al.* Identification of a multienzyme complex for glucose metabolism in living cells. *J. Biol. Chem.* **292,** 9191–9203 (2017).
20. Muddana, H. S., Sengupta, S., Mallouk, T. E., Sen, A. & Butler, P. J. Substrate catalysis enhance single-enzyme diffusion. *J. Am. Chem. Soc.* **132,** 2110–2111 (2010).
21. Riedel, C. *et al.* The heat released during catalytic turnover enhances the diffusion of an enzyme. *Nature* **517,** 227–230 (2015).
22. Illien, P. *et al.* Exothermicity is not a necessary condition for enhanced diffusion of enzymes. *Nano Lett.* **17,** 4415–4420 (2017).
23. Myers, T. C., Nakamura, K. & Flesher, J. W. Phosphonic acid analogs of nucleoside phosphate. I. The synthesis of 5′-adenylyl methylenediphosphate, a phosphonic acid analog of ATP. *J. Am. Chem. Soc.* **85,** 3292–3295 (1963).

24. Paduano, L., Sartorio, R., Errico, G. D. & Vitagliano, V. Mutual diffusion in aqueous solution of ethylene glycol oligomers at 25 °C. *J. Chem. Soc. Faraday Trans.* **94,** 2571–2576 (1998).
25. Annunziata, O. *et al.* Quaternary diffusion coefficients in a protein–polymer–salt–water system determined by Rayleigh interferometry. *J. Phys. Chem. B* **113,** 13446–13453 (2009).
26. Vergara, A., Paduano, L. & Sartorio, R. Mechanism of protein–poly(ethylene glycol) interaction from a diffusive point of view. *Macromolecules* **35,** 1389–1398 (2002).
27. Vanag, V. K. & Epstein, I. R. Cross-diffusion and pattern formation in reaction–diffusion systems. *Phys. Chem. Chem. Phys.* **11,** 897–912 (2009).
28. Schurr, J. M., Fujimoto, B. S., Huynh, L. & Chiu, D. T. A theory of macromolecular chemotaxis. *J. Phys. Chem. B* **117,** 7626–7652 (2013).
29. Wilkinson, K. D. & Rose, I. A. Isotope trapping studies of yeast hexokinase during steady state catalysis. A combined rapid quench and isotope trapping technique. *J. Biol. Chem.* **254,** 12567–12572 (1979).
30. Bermingham, A., Bottomley, J. R., Derrick, W. U. & Derrick, J. P. Equilibrium and kinetic studies of substrate binding to 6-hydroxymethyl-7,8-dihydropterin pyrophosphokinase from *Escherichia coli*. *J. Biol. Chem.* **275,** 17962–17967 (2000).
31. Wu, F., Pelster, L. N. & Minteer, S. D. Krebs cycle metabolon formation: metabolite concentration gradient enhanced compartmentation of sequential enzymes. *Chem. Commun.* **51,** 1244–1247 (2015).
32. Vopel, T. & Makhatadze, G. I. Enzyme activity in the crowded milieu. *PLoS ONE* **7,** e39418 (2012).
33. Baum, M., Erdel, F., Wachsmuth, M. & Rippe, K. Retrieving the intracellular topology from multi-scale protein mobility mapping in living cells. *Nat. Commun.* **5,** 4494 (2014).

Acknowledgements

The work was supported by Penn State MRSEC, funded by the National Science Foundation (NSF, DMR-1420620). P.J.B. acknowledges support from NSF CMMI 1334847. H.P. and H.H. acknowledge support by the Defense Threat Reduction Agency (award no. HDTRA1-14-1-0051).

Author contributions

M.K.G., P.J.B., H.H., S.J.B. and A.S. designed the research. X.Z., V.Y. and M.M.S. performed the experiments. H.P. performed the modelling. X.Z., H.P., V.Y., M.M.S., H.H., S.J.B. and A. S. analysed the data and wrote the manuscript. All authors contributed to the discussion of results.

Additional information

Supplementary information is available in the online version of the paper. Reprints and permissions information is available online at www.nature.com/reprints. Publisher's note: Springer Nature remains neutral with regard to jurisdictional claims in published maps and institutional affiliations. Correspondence and requests for materials should be addressed to H.H., S.J.B. and A.S.

Competing financial interests

M.K.G. has an equity interest in and is a cofounder and scientific advisor of VeraChem LLC.